Journal of Statistical Physics, Vol. 94, Nos. 3/4, 1999

The Ising Model on a Quenched Ensemble of $c = -5$ Gravity Graphs

K. N. Anagnostopoulos,[1] P. Bialas,[2] and G. Thorleifsson[3]

Received April 22, 1998; final September 21, 1998

We study with Monte Carlo methods an ensemble of $c = -5$ gravity graphs, generated by coupling a conformal field theory with central charge $c = -5$ to two-dimensional quantum gravity. We measure the fractal properties of the ensemble, such as the string susceptibility exponent γ_s and the intrinsic fractal dimension d_H. We find $\gamma_s = -1.5(1)$ and $d_H = 3.36(4)$, in reasonable agreement with theoretical predictions. In addition, we study the critical behavior of an Ising model on a *quenched* ensemble of the $c = -5$ graphs and show that it agrees, within numerical accuracy, with theoretical predictions for the critical behavior of an Ising model coupled *dynamically* to two-dimensional quantum gravity, with a total central charge of the matter sector $c = -5$.

KEY WORDS: Dynamical triangulations; quenched disorder; Ising model.

1. INTRODUCTION

Randomness in statistical systems arises in a variety of situations and is a very rich and complex subject. Quenched randomness is frequently used in studying the role of impurities and inhomogeneities in real physical systems where the characteristic time-scale of the disorder is much longer than other dynamics of the system. Annealed randomness, on the other hand, arises naturally in studies of fluctuating geometries, such as two-dimensional quantum gravity or fluid membranes, where the disorder is dynamically modified by interaction between the geometry and matter fields living on the surfaces.

For a statistical system coupled to random disorder, either in a quenched or annealed approach, the main question is to assess the effect

[1] The Niels Bohr Institute, DK-2200 Copenhagen, Denmark.
[2] Institute of Computer Science, Jagellonian University, 30-072 Krakow, Poland.
[3] Fakultät für Physik, Universität Bielefeld, D-33615 Bielefeld, Germany.

0022-4715/99/0200-0321$16.00/0

randomness has on the critical behavior of the pure system. One prediction in this direction is the Harris conjecture[1] which states that randomness changes the values of critical exponents only if the specific heat exponent α of the pure system is positive. This conjecture has been studied in many models with quenched disorder, such as the $2d$ Ising model[2] (where the Harris criterion is ambiguous as $\alpha = 0$) and the Potts model.[3] For both models a change in the critical behavior is observed.

All the above mentioned studies deal with weak disorder. More recently the critical behavior of systems on lattices with fractal structure very different from a flat surface has been investigated. Such systems arise naturally when matter, in the form of conformal field theories, is coupled to two-dimensional quantum gravity. These models can be studied either in a continuum formulation, by Liouville field theory, or using discretized approaches like, for example, models of dynamical triangulations, formulated either as matrix models or studied with numerical simulations. For these systems the disorder is, however, different from the one discussed above in that it is annealed, i.e., the models couple dynamically to fluctuations in the geometry.

A remarkable degree of universality does emerge for models coupled to two-dimensional quantum gravity. Namely, the change in the critical behavior of the systems, and their back-reaction on the geometry, only depends on the total central charge of the matter sector. This manifests itself in the so-called KPZ scaling relation which describe how the scaling dimensions of conformal operators are changed by the interaction with gravity.[4] Moreover, this universality also extents to the fractal structure of the surfaces, from which we derive the string susceptibility exponent γ_s and the fractal dimension d_H.

In view of this universality it is tempting to conjecture that the critical behavior of a particular system, when coupled to a fluctuating geometry, only depends on the (average) fractal structure of the surface. Details of the interaction between the system and the geometry, or the geometrical fluctuations, are not important as such—they only serve the purpose of defining the average fractal geometry. If this conjecture is true it implies that how the average over disorder is performed, i.e., that the disorder is annealed, is not essential. In particular, predictions of the KPZ scaling relation for the change in the critical behavior should just as well apply to models with quenched disorder, *provided the quenched average is taken over the same ensemble of disorder as is generated in the annealed approach.*

There are some recent simulations that have addressed the question of the critical behavior of spin models on a quenched ensemble of graphs generated by two-dimensional quantum gravity. Both the Ising model[5] and the 10-state Potts model[6] have been studied on an ensemble of pure

gravity graphs ($c = 0$). For the Ising model a critical behavior compatible with an Ising model coupled dynamically to gravity was found, although the accuracy of the results is not sufficient to rule out the conjecture discussed above.

The goal of this paper is two-fold. First, we want to investigate the fractal geometry of two-dimensional quantum gravity coupled to a conformal field theory with central charge $c = -5$. More precisely, we want to determine the fractal dimension of the corresponding surfaces, using recently developed finite-size scaling methods[7, 8] and to compare it to the (contradictory) theoretical predictions that exist.[9, 10] Second, we want to investigate the critical behavior of an Ising model on a quenched ensemble of $c = -5$ graphs and to compare it with predictions from Liouville theory, for the critical behavior of an Ising model coupled dynamically to two-dimensional quantum gravity. Our motivation for choosing $c = -5$ is that both its predicted fractal structure and the critical behavior of the Ising model is substantially different from both a flat space and for a pure two-dimensional quantum gravity. This makes these different critical behavior easier to distinguish in numerical simulations.

The paper is organized as follows: In Section 2 we study the fractal properties of a $c = -5$ conformal field theory coupled to two-dimensional gravity. We define the model in Section 2.1 and discuss the details of the simulations in Section 2.2. In Sections 2.3 and 2.4 we present our measurements of the string susceptibility exponent γ_s and of the fractal dimension d_H. And in Section 2.5 we comment on how this particular ensemble of graphs differs from other types of graphs frequently used in studying disordered system. The second part of the paper deals with an Ising model on the $c = -5$ graphs in a quenched approach. In Section 3.1 we discuss the prediction from Liouville theory for the critical behavior of an Ising model coupled dynamically to two-dimensional gravity. In Section 3.2 we discuss details of the simulations and the observables we use to probe the critical behavior. In Sections 3.3 and 3.4 we determine the critical temperature of the Ising model and the corresponding critical exponents. Finally, in Section 4 we summarize and discuss our results.

2. GEOMETRICAL PROPERTIES OF $c = -5$ GRAPHS

2.1. Dynamical Triangulations Coupled to Scalar Matter Fields

The model we study, and use to define our ensemble of random surfaces, is a discretization of a free bosonic string theory embedded in D-dimensions (for an excellent review see e.g., ref. 11). In the continuum formulation (Liouville theory) the partition function of two-dimensional

quantum gravity coupled to a conformal field theory, with central charge c, is defined as

$$Z(\bar{\mu}) = \int \mathscr{D}[g]\, \mathscr{D}\phi\, e^{-\bar{\mu} \int d^2\xi \sqrt{g} - S_M(\phi, g)} \tag{1}$$

where $\bar{\mu}$ is the cosmological constant, the integration is over equivalence classes of metrics $[g]$, and $S_M(\phi, g)$ is the matter Lagrangian. For a free bosonic string, embedded in D-dimensions, $S_M = (1/8\pi) \int d^2\xi \sqrt{g}\, g^{ab}\, \partial_a \vec{X}\, \partial_b \vec{X}$, where $\vec{X}$ are the embedding coordinates of the string.

Discretizing the model Eq. (1) using the simplicial gravity approach,[12] alias dynamical triangulations, the integration over metrics is replaced by a summation over all triangulations T constructed by gluing equilateral triangles together along their edges into a simplicial manifold of a given topology.[12] The discretized (grand-canonical) partition function becomes

$$Z(\mu) = \sum_A e^{-\mu A} \sum_{T \in \{\mathscr{T}\}} \int d[\mathbf{x}]\, \delta(\mathbf{x}_{cm})\, e^{-\sum_{\langle ij \rangle} (\mathbf{x}_i - \mathbf{x}_j)^2} \tag{2}$$

where A is the area of the triangulation (number of vertices), $\mathbf{x}$ is the embedding of a vertex in a D-dimensional space, and $\langle ij \rangle$ indicates that the sum is over adjacent vertices in the triangulation. The center of mass $\mathbf{x}_{cm}$ is kept fixed to eliminate the translational zero mode.

The integration over the Gaussian fields in Eq. (2) can be carried out explicitly and the canonical (fixed area) partition function becomes

$$Z_A = \sum_{T \in \mathscr{T}(A)} (\det C_T)^{-D/2} \tag{3}$$

where C_T is the adjacency matrix of the triangulation T:

$$C_T = \begin{cases} q_i & \text{if} \quad i = j \\ -c_{ij} & \text{if} \quad i \text{ and } j \text{ are adjacent} \\ 0 & \text{otherwise} \end{cases} \tag{4}$$

Here q_i is the order of vertex i and c_{ij} is the number of edges connecting the adjacent vertices i and j. Note that as we use degenerate triangulations, which are defined below, there can be more than two edges connecting the vertices i and j and the order of vertices is defined excluding self-loops. In calculating the determinant of C_T one vertex is excluded from the graph in order to eliminate the zero mode.

In the partition function Eq. (3) the embedding dimension D now appears as a free parameter and is no longer restricted to positive integer values. In particular, it can be taken to be negative; this corresponds to coupling a conformal field theory with a negative central charge $c = D$ to two-dimensional gravity.

The sum over triangulations T in Eq. (2) is over an appropriate class of triangulations $\mathscr{T}$ of area A and with fixed topology. Different classes amount to different discretization of the manifolds. By universality arguments different choices of $\mathscr{T}$ should yield the same critical behavior as long as they only differ at the level of the discretization. This statement is known to be true for two commonly used classes of triangulations, *degenerate* ($\mathscr{T}_D$) and *combinatorial* ($\mathscr{T}_C$) triangulations. Combinatorial triangulations are defined by forbidding self-loops (an edge starting and ending at the same vertex) and vertices connected by more than one edge. These pathologies are, on the other hand, allowed in the class of degenerate triangulations. For these particular classes of triangulations the model Eq. (2) has been solved for some special values of c.[13] This universality holds even if curvature fluctuations of the triangulation, i.e., the vertex orders q_i, are maximally restricted, to $q_i = 6 \pm 1$, as shown by numerical simulations.[14]

Finite-size effects do, however, depend on the discretization; in particular, for degenerate triangulations they are substantially smaller (one order of magnitude) than for combinatorial.[15] In the work presented in this paper we use degenerate triangulations of spherical topology.

It is possible to get some insight into the behavior of the model in the limits $D \to \pm\infty$ by looking at what triangulations dominate the sum in Eq. (3).[16] As the determinant of C_T is related to the number of spanning trees on a particular graph, the graphs dominating in the limit $D \to +\infty$ are those with a minimal number of spanning trees. This corresponds to triangulations with a branched polymer structure. In the limit $c \to -\infty$, on the other hand, we expect the determinant C_T to take its largest value for triangulations with a maximal number of spanning trees. This implies that the dominant triangulations in this limit will be flat with $q_i = 6$ (apart from few defects $q_i \neq 6$ needed to form a closed spherical surface).

2.2. Simulating a $c = -5$ Gravity Theory

We have studied numerically the partition function Eq. (3) for $c = -5$ using Monte Carlo simulations. The space of all triangulations is explored using the so-called edge-flip algorithm[16] in which an edge l_{ij}, common to two triangles t_{ijh} and t_{kji}, is removed (or flipped) and replaced by the edge

l_{hk}. This algorithm is known to be ergodic (for fixed area). Unfortunately, the determinant in Eq. (3) corresponds to a non-local action making the simulations very difficult. Every time a flip of an edge is proposed the whole determinant has to be recalculated, an operation requiring on the order of N^3 floating point operations. We can exploit the locality of the flip and using standard techniques[17] to reduce this to N^2 floating point operations per flip, but this still limited our simulations to triangulations consisting of up to 1600 vertices. Nevertheless, those triangulations are considerably larger than have been simulated before with this method.[18]

In the simulations we stored triangulations after every 10 to 20 Monte Carlo sweeps, were each sweep consisted of flipping, approximately, an area worth of edges. With the auto-correlations present, which are relatively modest on such small surfaces, the stored graphs were more or less independent. In Table 1 we show the total number of graphs we generated, and analyzed, for each area.

2.3. The String Susceptibility Exponent γ_s

To determine the critical behavior of the model Eq. (3), with $c = -5$, we measured two critical exponents: the *string susceptibility* exponent γ_s and the *fractal* or Hausdorff dimension d_H. The latter will be discussed in the next section, here we consider γ_s.

Table 1. The Number N_g of $c = -5$ Graphs of Area A Generated by Simulating the Model Equation (3)[a]

A	N_g	N_r
100	3000	200
150	3000	
200	3000	200
300	3000	
400	2000	130
600	2500	
800	700	60
1200	196	178
1600	96	96

[a] Also shown is the number N_r of different replicas (graphs), for each area, on which we simulated the Ising model (Section 3).

The string susceptibility exponent is defined by the singular behavior of the grand-canonical partition function Eq. (2) as the cosmological constant μ approaches its critical value:

$$Z(\mu) \approx Z_{\text{reg}} + (\mu - \mu_c)^{2-\gamma_s} \tag{5}$$

This implies that the canonical partition function behaves asymptotically as

$$Z(A) \sim e^{\mu_c A} A^{\gamma_s - 3}, \qquad A \to \infty \tag{6}$$

The value of γ_s can be calculated from the Liouville field theory:[4]

$$\gamma_s = \tfrac{1}{12}(c - 1 - \sqrt{(c-25)(c-1)}) \tag{7}$$

For $c > 1$ this implies a complex critical exponent and the corresponding theory is not well defined—this is related to the existence of tachyons in string theories in embedding dimension larger than two. For $c \leqslant 1$, on the other hand, the theory is well defined and, specifically, for $c = -5$ Eq. (7) predicts $\gamma_s = -1.618\ldots$

In order to measure γ_s for the ensemble of triangulations, generated in our simulations, we study the distribution of so-called *minbus* (minimal neck baby universes).[19] A minbu is a part of the triangulation connected to the rest through a minimal neck; for a degenerate triangulation a minimal neck is simply a self-loop. By counting in how many ways a minbu of size B can be connected to a surface of size $(A - B)$, the size distribution of minbus can be written as:

$$n_A(B) = \frac{B\, Z(B)(A-B)\, Z(A-B)}{Z(A)} \tag{8}$$

$$\sim [(A-B)\, B]^{\gamma_s - 2} \tag{9}$$

In the last step we have used the asymptotic behavior of the partition function, Eq. (6)—in this way the leading exponential behavior cancels out and we can directly access the sub-leading corrections governed by γ_s.

The distribution $n_A(B)$ is easily measured in numerical simulations and γ_s extracted by a fit to Eq. (9). In practice, though, one has to impose a lower cut-off on the size of minbus included in the fit as there are finite-size corrections to the asymptotic form Eq. (6). This can be done in a systematic way; small minbus are thrown away in the fitting procedure until one gets a stable value of γ_s and an acceptable χ^2-value for the fit.[20] Unfortunately, the large negative value of γ_s for the $c = -5$ graphs makes this measurements more difficult than for previously studied ensembles of triangulations, as the distribution falls off very rapidly.

We have measured γ_s for surfaces of area up to 300 vertices; for the larger surfaces our statistics was not sufficient for a reliable determination of the minbu distribution. Although these are very small surfaces, our experience in measuring γ_s for other models of dynamical triangulations shows that they are large enough, provided one is using degenerate triangulations.[15] In this particular case the lack of statistics is much more of a problem than the smallness of the triangulations. But as determining γ_s is of secondary interest for us, we did not deem it worthwhile to invest too much CPU-power in increasing the statistics. We get the following values of γ_s:

A	γ_s
100	$-1.52(17)$
150	$-1.42(15)$
200	$-1.37(22)$
300	$-1.71(19)$

Those values are in reasonable agreement with the theoretical value $\gamma_s = -1.618\ldots$

2.4. The Vertex–Vertex Correlation Function and d_H

Another exponent that characterizes the fractal structure of the surfaces is the (intrinsic) fractal dimension d_H. It can be defined from the behavior of the vertex–vertex (or two-point) correlation function $g_A(r)$:

$$g_A(r) = \frac{1}{A} \left\langle \sum_{i,j} \delta(d_{ij} - r) \right\rangle_T \tag{10}$$

where d_{ij} is the (minimal) geodesic distance between two vertices i and j and the statistical average is performed over all triangulations T. This correlation function simply counts the number of vertices (or the area of the manifold) at a geodesic distance r from a marked vertex i, averaged over all vertices i. We expect its short distance behavior to be $g_A(r) \sim r^{d_H - 1}$, provided $r \ll A^{1/d_H}$.

On a triangulation we define the geodesic distance between two vertices as the shortest path between them traversed along links. Alternatively, one can define a triangle–triangle correlation function $t_A(r)$, analogous to Eq. (10), in which case the geodesic distance is defined as the shortest path between two triangles traversed through the center of triangles. Although those two definitions will result in very different correlation functions for a particular triangulation, they should define the same fractal dimension.

To extract the fractal dimension from the measurements of the correlation function Eq. (10) it is convenient to use methods of finite-size scaling. Assuming that the only relevant length-scale in the model is defined by A^{1/d_H}, general scaling arguments[7, 8] imply that

$$g_A(r) \sim A^{1-1/d_H} F(x) \tag{11}$$

where we have introduced the scaling variable

$$x = \frac{r}{A^{1/d_H}} \tag{12}$$

In fixing the prefactor in Eq. (11) we have used that $\sum_r g_A(r) = A$.

In practice there are strong finite-size corrections to this scaling behavior. The measurements of d_H can be improved, considerably, by including the simplest finite-size correction to x, i.e., by introducing the so-called *shift*:[8]

$$x = \frac{r+a}{A^{1/d_H}} \tag{13}$$

where the shift parameter a will in general depend on the particular observable we consider. This scaling correction has been applied successfully to all geometric and matter correlation functions, even with quite different functional dependence on x.[21] Its possible geometric origin has been investigated analytically for $c = 0$ in ref. 22. The shift was also found and calculated analytically in correlation functions on branched polymers where it has been shown to contain the singularity responsible for the crumpling phase transition.[23]

It is possible to generalize Eq. (10) to higher moments of the correlation function. Introducing the loop-length distribution $\rho_A(r, l)$, which counts the number of loops of length l at geodesic distance r from a marked vertex i, we define the k-th moment of l as[10, 21, 22]

$$l_A^k(r) = \sum_l l^k \rho_A(r, l) \tag{14}$$

Note that $g_A(r) = l_A^1(r)$. On a triangulation loops are defined as a connected (by links) subset of the vertices that are at distance r from i.[4] However, the

[4] In a similar way we can define a loop-length distribution for the triangles at a distance r from a marked triangle. In that case we define a loop as a connected subset of triangles sharing at least one vertex. If we define loops as triangles sharing at least one link, then those loops always stay at the level of the lattice cut-off.

generalization of the scaling hypothesis Eq. (11) is more subtle, as it depends on how the boundary length l scales with the radius r.[22] If we assume that $\dim[r^2] \equiv \dim[l] = \dim[A^{2/d_H}]$, then we have for the moments:

$$l_A^k(r) = A^{2k/d_H} F_k(x), \qquad k > 1 \tag{15}$$

Alternatively, if we assume that $\dim[l^2] \equiv \dim[A] = \dim[r^{d_H}]$, we get:

$$l_A^k(r) = A^{k/2} \tilde{F}_k(x) \tag{16}$$

Our measurements clearly favor the former scaling form Eq. (15); this is compatible with results recently obtained for a $c = -2$ theory.[22] This implies, from dimensional analysis, that the boundary length l acquires an anomalous scaling dimension with the area; at present the origin of this behavior is still not understood. Note that in the only soluble case, $c = 0$, both scaling forms agree.

We have measured the moments $l_A^k(r)$ for $k \leqslant 4$, together with the triangle–triangle correlation function $t_A(r)$. The scaling behavior, Eqs. (11) and (15), is analyzed by "collapsing" the distributions corresponding to different area onto a single curve. For this purpose it is convenient to interpolate between the (discrete) values of x—this we do using a cubic-spline (see ref. 22 for details). The collapse depends on only two free parameters, a and d_H; their optimal values are determined by minimizing the χ^2-value for the collapse, where the χ^2-value is defined by the difference between the curves after rescaling. The results are shown in Table 2. We used triangulations of area 200 to 1600 in the analysis; if we included smaller graphs it

Table 2. The Fractal Dimension d_H for an Ensemble of $c = -5$ Graphs Determined by Collapsing the Correlation Functions $l_A^k(r)$ onto a Single Curve Using the Scaling Forms (11) and (15) and the Shift (13)[a]

$l_A^k(r)$	k	d_H	a
$g_A(r)$	1	3.36(16)	0.6(6)
	2	3.33(5)	0.4(3)
	3	3.36(4)	0.4(3)
	4	3.36(4)	0.4(3)
$t_A(r)$		3.07(24)	2.4(1.6)

[a] The corresponding (optimal) value of the shift parameter a is included. Graphs of area 200 to 1600 were included in the analysis. The corresponding values for the triangle–triangle correlation function $t_A(r)$ are also included.

was not possible to get an acceptable χ^2-value for the fit. We observe, as has been observed before,[7, 8] that the finite-size effects are considerable bigger for the triangle–triangle correlation function. This is also reflected in much larger value of the shift parameter a.

To demonstrate how good this scaling behavior actually is, we show in Fig. 1 the scaled curves for the vertex–vertex correlation function $g_A(r)$. These curves have been scaled using $d_H = 3.36(4)$, the average value of the fractal dimension from Table 2, and the corresponding value of the shift. The quality of the scaling for the higher moments, and for $t_A(r)$, is equally impressive.

Finally, we look at the loop-length distribution $\rho_A(r, l)$. Although, in principle, it contains the complete set of informations about the moments, it is not very convenient for extracting the fractal dimension. Nevertheless, we demonstrate that its scaling behavior is consistent with the measured fractal dimension. Since our measurements show that for the higher moments $l \sim r^2$ (see Eq. (15)), i.e., the same behavior as for $c = 0$, we expect that

$$\rho_A(r, l) \approx r^2 F_\rho(l/r^2) \tag{17}$$

We show an example of this scaling in Fig. 2. The relation Eq. (17) is, of course, exact only for $\rho_\infty(r, l)$, as is the case for $c = 0$,[10] and finite-size effects are expected for small l/r^2. The deviation from the above scaling behavior is, in principle, determined by the scaling corrections Eqs. (11) and (15).[21]

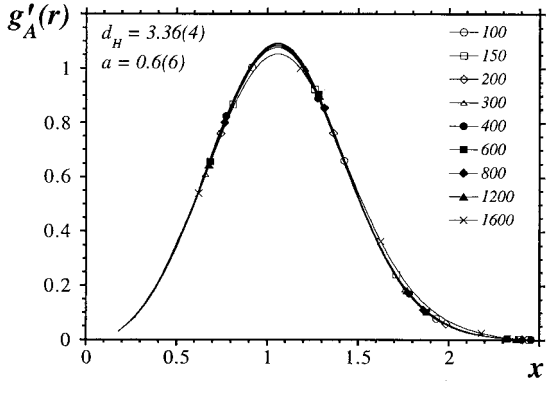

Fig. 1. The scaled vertex–vertex correlation function $g'_A(r) \equiv g_A(r)/A^{1-1/d_H}$ vs. the scaling variable $x = (r + a)/A^{1/d_H}$. The measured value of the fractal dimension $d_H = 3.36$ and a shift $a = 0.6$ were used in the scaling.

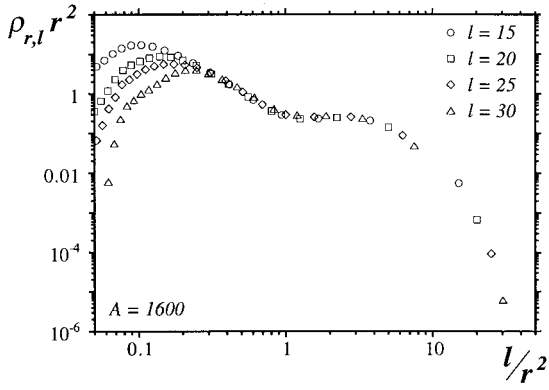

Fig. 2. An example of the scaling behavior of the loop-length distribution function $\rho_A(r, l)$ for $A = 1600$. The distributions for different choices of l are re-scaled in accordance with Eq. (17).

As we mentioned in the Introduction, there exist several theoretical predictions for the fractal dimension for theories of two-dimensional quantum gravity coupled to matter. Using string field theory, or a transfer matrix approach, with a modified definition of a geodesic distance, one gets:[9]

$$d_H = \frac{2}{|\gamma_s|} = \frac{24}{1 - c + \sqrt{(25 - c)(1 - c)}} \tag{18}$$

An alternative expression is obtained by studying the diffusion on the surface, within the framework of Liouville theory:[10]

$$d_H = 2 \times \frac{\sqrt{25 - c} + \sqrt{49 - c}}{\sqrt{25 - c} + \sqrt{1 - c}} \tag{19}$$

These two analytical predictions disagree, except in the case of pure gravity; the only case where an exact solution exist.[24] For $c = 0$ we have $d_H = 4$, this value is also obtained in numerical simulations using the scaling methods described above.[7, 8] On the other hand, both Eqs. (18) and (19) disagree with the results of extensive numerical simulations of conformal field theories with $0 < c \leqslant 1$ coupled to gravity.[7, 8, 25, 21] The numerical simulations indicate that the fractal dimension is 4 independent of the coupling to matter. In ref. 26, the discrepancy for $c = 1/2$—one Ising model coupled to gravity—has been attributed to the subtlety in how the continuum limit should be taken in this model. An alternative proposal has been made in ref. 27 where the authors suggest that a different scaling

variable, related to the size of clusters, should be used in the derivation of Eq. (18) instead of the geodesic distance. It should be emphasized, however, that the present numerical accuracy is not enough to rule out completely the prediction of Eq. (19) for $c > 0$.

The only model with $c < 0$ where the fractal dimension has been measured numerically is $c = -2$ or topological gravity.[22] This is a very special case were it is possible to sample the space of triangulations recursively; this allows simulations of very large graphs (graphs of up to 8×10^6 triangles were used in ref. 22). The measured fractal dimension in this case is $d_H = 3.58(4)$, which agrees very well with the prediction from Liouville theory, Eq. (19): $d_H = 3.561\ldots$

Our result for $c = -5$, $d_H = 3.36(4)$, also agrees reasonably well with Eq. (19), which predicts $d_H = 3.236\ldots$ for $c = -5$, especially given the smallness of our graphs. On the other hand, it completely rules out the prediction of Eq. (18): $d_H \approx 1.236$. Although the value 3.36(4) is slightly larger than predicted by Eq. (19), we notice that the fractal dimension obtained using the triangle–triangle correlation function: $d_H = 3.07(24)$, is somewhat smaller. This effect was also noticed for the $c = -2$ model where the two values converged to Eq. (18) on larger graphs. This is what we observe in our simulations as well.

2.5. Comparison with Other Random Lattices

The fractal structure of the $c = -5$ graphs differ substantially from other types of random lattices frequently studied. An ensemble of random lattices, commonly used in the study of quenched disorder, is Poissonian random lattices. They are constructed by distributing vertices uniformly on a two-dimensional manifold and link them together to form a triangulation, usually following a prescription by Dirichlet and Voronoi.[28]

We have compared the properties of our ensemble of graphs to that of Voronoi triangulations by looking at the probability distribution of vertex orders p_n. In Fig. 3 we plot this distribution for the $c = -5$ graphs, Voronoi triangulations, and, for comparison, pure gravity ($c = 0$) and branched polymer ($c = 5$) graphs. As in all cases the distributions are for triangulations, they all have the mean value $\bar{p}_n = 6$, but in other aspects they differ. The distribution for Voronoi graphs is peaked sharply around the mean value and falls off rapidly as n increases. The pure gravity distribution peaks at the smallest possible curvature ($n = 1$ for degenerate triangulations) and falls off much slower. The distribution for $c = -5$ lies in-between, as could be expected from its fractal dimension.[5]

[5] It is worth noting that the fractal dimension alone is not enough to characterize the graphs. For example, both a flat lattice and branched polymers have $d_H = 2$.

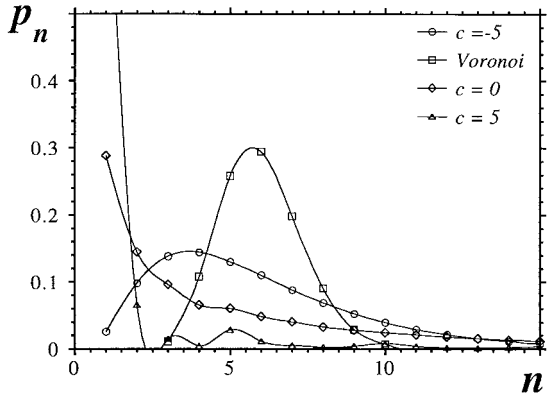

Fig. 3. The (normalized) curvature distribution p_n for an ensemble of graphs corresponding to $2d$-gravity coupled to matter with $c = -5$, 0 and 5, respectively, and for Voronoi triangulations. The interpolating curves are just to guide the eye.

As Fig. 3 indicates, the randomness of the Voronoi triangulations is only at the local level, their global fractal structure, defined by, for example, the fractal dimension or the string susceptibility exponent, will be the same as of the underlying two-dimensional flat lattice used in constructing them. In this respect their randomness is only a (small) local perturbation around the flat background. This is also reflected in that the critical behavior of spin models on such triangulations is the same as for a flat lattice.[29] This is contrary to the other ensembles of graphs shown in Fig. 3, which have a genuinely different global fractal structure.

It should also be emphasized that although local observables such as p_n reveal something about the randomness of the graphs, they are not a universal property and not a good indicator for the critical behavior of the corresponding model. Within the context of $2d$ gravity the local properties of a given model can be changed by adding an irrelevant operator to the action in Eq. (2); for example, a term that couples to the local curvature. But, except in extreme cases, this modification does not affect the critical behavior of the model.[14, 30]

It is, however, possible to change the global fractal properties of the graphs defined by the $2d$-gravity model Eq. (3) by adjusting the embedding dimension D. In particular, by taking D negative we can create an ensemble of triangulations with any fractal dimension between 2 and 4. This makes the model of Eq. (3) ideal for investigating how the fractal properties, like the fractal dimension, affect the critical behavior of a spin model living on the graphs. As will be demonstrated in the next section, in the case of the

Ising model this results in critical exponents that are radically different from those of the Ising model on a flat lattice.

3. THE ISING MODEL ON $c = -5$ GRAPHS

3.1. Predictions from the Continuum

In this second part of the paper we investigate how the critical behavior of an Ising model is modified when it is defined on a quenched ensemble of $c = -5$ graphs. In the annealed case coupling a conformal field theory to $2d$-gravity results in dressing the dimensions of primary operators of the theory. The dressed weights are given by the KPZ formula.[4] From those weights one can calculate the new critical exponents. As a dynamical triangulation, the only case that has been solved explicitly is the one Ising model coupled to gravity, formulated as a two-matrix model.[13] In that case the phase transition changes from second to third order and the critical exponents agree with the ones calculated using the KPZ formula.

All these calculations are, as emphasized above, for the Ising model on an annealed ensemble of graphs. Now the conjecture, discussed in the Introduction, is that the interaction between the Ising model and the geometry is not important; the critical behavior is simply determined by the average fractal structure of the triangulations. This implies that we can also use the KPZ formula to calculate the critical behavior for an Ising model on a quenched ensemble of graphs, provided they define the appropriate fractal structure. If the conjecture is true the critical behavior of an Ising model on a quenched ensemble of $c = -5$ graphs is the same as that of the Ising model coupled dynamically to gravity with additional $c = -11/2$ conformal field coupled to it.

Given a primary operator of conformal weight Δ^0 in the original theory, the KPZ formula gives its conformal weight after coupling to gravity:

$$\Delta = 2 \times \frac{\sqrt{1 - c + 12\Delta^0} - \sqrt{1 - c}}{\sqrt{25 - c} - \sqrt{1 - c}} \tag{20}$$

For the Ising model the relevant operators are the energy density ε and the spin σ; from the conformal weight of those operators we can calculate the specific heat exponent α and the magnetization exponent β:

$$\alpha = \frac{2(1 - \Delta_\varepsilon)}{2 - \Delta_\varepsilon} \qquad \text{and} \qquad \beta = \frac{\Delta_\sigma}{2 - \Delta_\varepsilon} \tag{21}$$

In flat space the conformal weights of the Ising operators are: $\Delta_\varepsilon^0 = 1$ and $\Delta_\sigma^0 = 1/8$; hence the KPZ formula, together with Eq. (21), predicts $\alpha \approx -0.452432$ and $\beta \approx 0.234186$ for an Ising model on $c = -5$ graphs. The full list of exponents is shown in Table 5. As those exponents are very different from both the Ising model exponents on a flat lattice (the Onsager exponents) and coupled dynamically to pure gravity (both sets of exponents are included in the table) it should be relatively easy to distinguish them in numerical simulations.

3.2. The Ising Model Simulations

We have simulated the Ising model for several independent replicas of the $c = -5$ graphs we generated. We did this for graphs of size 100, 200, 400, 800, 1200 and 1600 vertices—for the number of replicas we sampled see Table 1. We use the standard definition of the Ising model:

$$Z_{\text{Ising}}(T) = \sum_{\{\sigma_i\}} e^{\beta \sum_{\langle ij \rangle} \sigma_i \sigma_j} \tag{22}$$

where $\sigma_i = \pm 1$ and $\langle ij \rangle$ denotes adjacent vertices in the graph T. The Ising spins are placed on the vertices of the graphs; alternatively they could be put on the triangles, but based on duality arguments we would expect the same critical behavior (this is the case for an Ising model coupled dynamically to $2d$-gravity[13]). Naively, one might expect that placing the spins on the triangles was preferable as for a graph of a given area this yield twice as many spins. But as the finite-size effects are dominated by the geometry not the number of spins this not the case. In fact, it would only increase the computational efforts in updating the spin configuration.

We simulated at several values of the inverse temperature $\beta = J/k_B T$ for $\beta \in [0.15, 0.25]$. A Swendsen–Wang cluster algorithm was used to update the spin configuration and typically about 200.000 measurements taken at each β value; the measurements were separated by 10 to 20 cluster updates. For each measurement we stored the total energy of the system, $E = \sum_{\langle ij \rangle} \sigma_i \sigma_j$, and the magnetization, $M = \sum_i \sigma_i$; all other observables can be constructed from the those two. To interpolate between measurements at different temperatures we used standard multi-histogram methods.[31]

All observables $\mathcal{O}$ were calculated for each replica independently and the average over the different replicas r performed afterwards:

$$\bar{\mathcal{O}} = \frac{1}{N_r} \sum_r \mathcal{O}_r \tag{23}$$

This is in accordance with the philosophy that the quenched average should be performed at the level of the free energy, *not* at the level of the partition function.[32] The error on $\bar{\mathcal{O}}$ is estimated by a jackknife analysis over different replicas.

To analyze the critical behavior of the Ising model we constructed several standard observables. In addition to the energy density $\langle e \rangle$ and magnetization $\langle m \rangle$ per vertex we considered:

$$\begin{aligned}
C_A &= \beta^2 A(\langle e^2 \rangle - \langle e \rangle^2) \approx c_0 + c_1 A^{\alpha/\nu d_H} && \text{(specific heat)} \\
\chi &= A(\langle m^2 \rangle - \langle m \rangle^2) \sim A^{\gamma/\nu d_H} && \text{(magnetic suscept.)} \\
U_A &= \frac{\langle m \rangle^4}{\langle m^2 \rangle^2} \approx c_0' && \text{(Binder's cumulant)} \\
V_A &= \frac{\langle e \rangle^4}{\langle e^2 \rangle^2} && \text{(energy cumulant)}
\end{aligned} \tag{24}$$

together with the various derivatives of the magnetization:

$$\begin{aligned}
\mathrm{D}_{|m|} &\equiv \frac{\mathrm{d}\langle |m| \rangle}{\mathrm{d}\beta} = A(\langle e \rangle \langle m \rangle - \langle e\, |m| \rangle) \sim A^{(1-\beta)/\nu d_H} \\
\mathrm{D}_{\ln |m|} &\equiv \frac{\mathrm{d} \ln \langle |m| \rangle}{\mathrm{d}\beta} = A\left(\langle e \rangle - \frac{\langle e\, |m| \rangle}{\langle |m| \rangle} \right) \sim A^{1/\nu d_H} \\
\mathrm{D}_{\ln m^2} &\equiv \frac{\mathrm{d} \ln \langle m^2 \rangle}{\mathrm{d}\beta} = A\left(\langle e \rangle - \frac{\langle e m^2 \rangle}{\langle m^2 \rangle} \right) \sim A^{1/\nu d_H} \\
\mathrm{D}_{U_A} &\equiv \frac{\mathrm{d} U_A}{\mathrm{d}\beta} = A(1 - U_A)\left(\langle e \rangle - 2\frac{\langle m^2 e \rangle}{\langle m^2 \rangle} + \frac{\langle m^4 e \rangle}{\langle m^4 \rangle} \right) \sim A^{1/\nu d_H}
\end{aligned} \tag{25}$$

In Eqs. (24) and (25) we have included the expected finite-size scaling behavior. For some of the observables this scaling behavior applies both at the infinite-area critical temperature $\bar{\beta}_c$ and to the scaling of their extremal values.

3.3. The Critical Temperature $\bar{\beta}_c$

To determine the critical temperature $\bar{\beta}_c$ we use that the pseudo-critical temperature $\bar{\beta}_c(A)$, defined by the location of peaks in the different observables, approaches the infinite-area value like:

$$\bar{\beta}_c(A) \approx \bar{\beta}_c + \frac{c_0}{A^{1/\nu d_H}} \tag{26}$$

The observables we have used for this purpose are: $\bar{C}_A$, $\bar{\chi}$, $\bar{\mathrm{D}}_{|m|}$, $\bar{\mathrm{D}}_{\ln|m|}$, $\bar{\mathrm{D}}_{\ln m^2}$, and $\bar{\mathrm{D}}_{U_A}$, all of which have well resolved peaks. An example of this is shown in Fig. 4 were we plot the specific heat and the magnetic susceptibility. In the figure the curves shown are the averages over different replicas of the model, Eq. (23). To determine $\bar{\beta}_c(A)$, and to estimate the corresponding error, we locate the peaks on each replica independently and then take the averages over the replicas. In the infinite-area limit, were one expects the triangulations to become self-averaging with respect to the fractal structure, the distribution of $\beta_c^r(A)$ should approach a delta-function

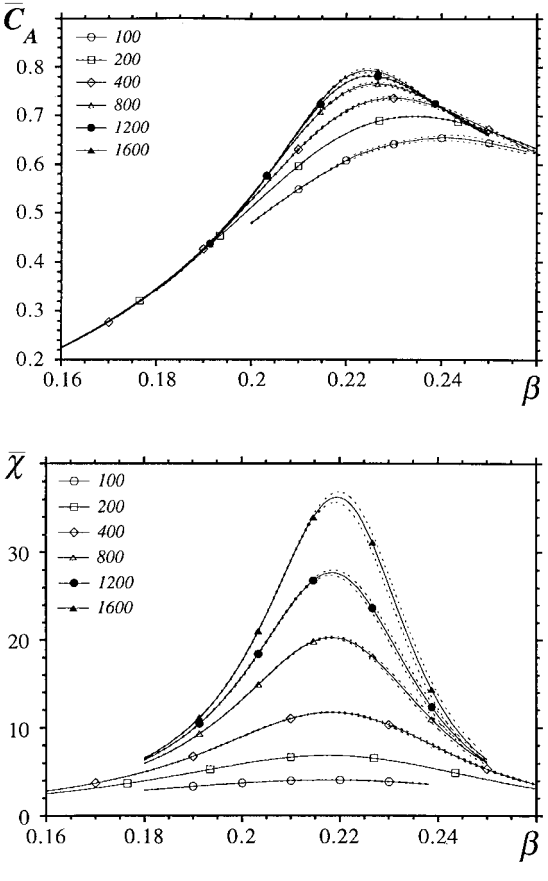

Fig. 4. (a) The specific heat $\bar{C}_A$ for an Ising model on an ensemble of quenched $c = -5$ graphs. (b) The corresponding magnetic susceptibility $\bar{\chi}$. For both observables the curves, for each area A, are the averages over different replicas and the errors (dashed lines) are estimated using jack-knifing over replicas.

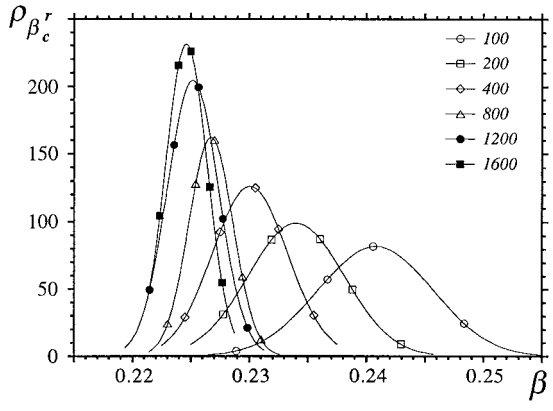

Fig. 5. Fits of the (normalized) distributions of the pseudo-critical temperature $\beta_c^r(A)$ to a Gaussian distribution: $\rho(\beta_c^r) = a \exp(-(\beta_c^r - \bar{\beta}_c)^2/b)$. This is for $\beta_c^r(A)$ defined by peaks in the specific heat C_A^r, for an Ising model simulated on different replicas r of $c = -5$ graphs. Note that the symbols are only to identify distributions corresponding to different area.

centered at $\bar{\beta}_c$. This we demonstrate in Fig. 5 where we show the (normalized) distributions of pseudo-critical temperatures $\rho(\beta_c^r)$; in this case for the specific heat. And, indeed, the distributions get narrower as the area is increased. Similar behavior is observed for the other observables.

The fit to Eq. (26) is made considerably easier by an independent determination of the critical exponent vd_H. The peak values of the

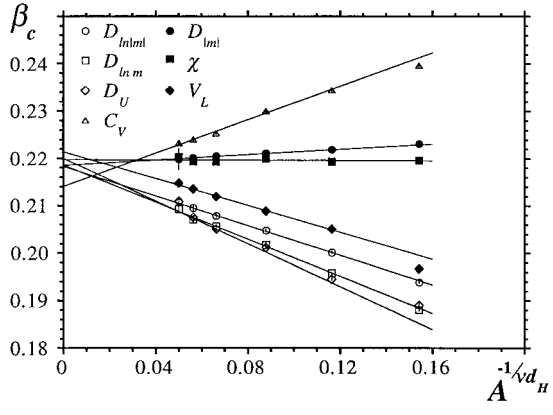

Fig. 6. Scaling of the pseudo-critical temperature $\bar{\beta}_c(A)$ vs. the scaled area A^{-1/vd_H}, using $vd_H = 2.464$. This is shown for all the different observables we considered. The approach to the (infinite-area) critical temperature $\bar{\beta}_c$ is demonstrated by a linear fit to Eq. (26) (excluding the smallest system size).

derivatives $\bar{\mathrm{D}}_{\ln|m|}$, $\bar{\mathrm{D}}_{\ln m^2}$, and $\bar{\mathrm{D}}_{U_A}$ all scale like $A^{1/\nu d_H}$. We have used this to determine νd_H by a linear fit; those exponents are shown in Table 4 and the corresponding fits in Fig. 6. To demonstrate the finite-size effects we have done the fits with both $A_m = 100$ and $A_m = 200$ as the smallest area included in the fit. Although the exponents are not substantially altered by excluding graphs of area 100, for most observables the χ^2-value of the fit is, however, unacceptably large if they are included.

Using the average value $\nu d_H = 2.464(19)$, we obtain the critical temperature from a linear fit to Eq. (26). The result, for the different observables we considered, is shown in Table 3. This yields the average value $\bar{\beta}_c = 0.2187(9)$ (using $A_m = 200$).

3.4. The Critical Exponents

We then proceed to determine the critical exponents of the model by fitting the different observables to their expected finite-size scaling behavior, Eqs. (24) and (25), both at the critical temperature and, were appropriate, also their peak values. The exponents, obtained from those fits, are collected in Table 4.

The exponents have been determined both for $A_m = 200$ and 400, except for the specific heat which is the most difficult quantity to analyze. It requires a nonlinear 3-parameter fit to the scaling behavior Eq. (24) and, in addition, as it does not diverge for this particular model the regular

Table 3. The Critical Temperature $\bar{\beta}_c$ for the Ising Model on $c = -5$ Graphs Determined from the Scaling of the Location of Peaks in the Different Observables[a]

	$A \in \{100, 1600\}$		$A \in \{200, 1600\}$	
$\bar{\mathcal{O}}$	$\bar{\beta}_c$	χ^2	$\bar{\beta}_c$	χ^2
$\bar{C}_A$	0.2153(15)	19	0.2140(17)	7.9
$\bar{\chi}$	0.2197(11)	6.7	0.2197(16)	7.9
$\bar{U}_A$	0.2233(12)	5.6	0.2214(10)	2.1
$\bar{\mathrm{D}}_{\ln\|m\|}$	0.2187(5)	1.3	0.2183(7)	0.8
$\bar{\mathrm{D}}_{\ln m^2}$	0.2188(7)	4.5	0.2186(10)	4.0
$\bar{\mathrm{D}}_{\|m\|}$	0.2184(5)	0.3	0.2185(4)	0.1
$\bar{\mathrm{D}}_{U_N}$	0.2188(22)	15	0.2200(13)	2.0
Average	0.2188(9)		0.2187(9)	

[a] This is for both $A_m = 100$ and 200 as the smallest area include in the linear fit to Eq. (26). Also included is the χ^2-value (per d.o.f.) for the fits.

Table 4. The Critical Exponents of the Ising Model on a Quenched Ensemble of $c = -5$ Graphs Determined from the Scaling of Various Observables Both at the Critical Temperature $\bar{\beta}_c \approx 0.2187$ and, Where Appropriate, of Peak Values[a]

		(A) Scaling of peaks				(B) Scaling at $\bar{\beta}_c$			
	$\bar{\mathcal{O}}$	$A_m = 200$	χ^2	$A_m = 400$	χ^2	$A_m = 200$	χ^2	$A_m = 400$	χ^2
vd_H	$\bar{\mathrm{D}}_{\ln \lvert m \rvert}$	2.414(20)	7.8	2.469(37)	2.3	2.413(15)	1.0	2.451(28)	0.4
	$\bar{\mathrm{D}}_{\ln m^2}$	2.405(23)	9.4	2.456(23)	1.3	2.399(22)	2.4	2.431(35)	0.9
	$\bar{\mathrm{D}}_{U_N}$	2.591(43)	2.4	2.528(72)	1.7	2.50(12)	4.3	2.45(11)	3.3
β/vd_H	$\lvert m \rvert$					0.1055(34)	3.0	0.1006(67)	0.5
	$\bar{\mathrm{D}}_{\lvert m \rvert}$	0.1001(69)	1.3	0.1070(58)	0.1	0.0967(52)	2.5	0.1064(79)	1.0
γ/vd_H	$\bar{\chi}$	0.7966(31)	2.9	0.7922(99)	2.6	0.7825(57)	6.8	0.7958(146)	4.0
α/vd_H	$\bar{C}_A$	−0.266(90)	0.7			−0.269(78)	0.4		

[a] Graphs of area $A \geqslant A_m$, with $A_m = 200$ and 400, are included in the fits to Eqs. (24) and (25) (except for $\bar{C}_A$ where it was not possible to obtained a reliable fit if area 200 was excluded).

background term is all the more important. Thus we could not get a stable fit if we excluded graphs smaller that 400 and, as is apparent from the quoted errors, the estimate of this exponent is the least reliable. On the other hand, for the other exponents, most determined from more that one observable, we get very consistent estimates. In all cases graphs of area 100 had to be excluded in order to obtain an acceptable fit.

Although the triangulations we have employed in this study are smaller than those usually used in simulations of two-dimensional gravity—due to the difficulty in simulating the non-local action Eq. (3)—this is to a large extent compensated by a smaller fractal dimension, which sets the relevant length-scale that controls the finite-size effects. Hence we are able to obtain reliable estimates of the critical exponents, even from graphs of such modest size.

We have collected in Table 5 our numerical estimates of the exponents of an Ising model on a quenched ensemble of $c = -5$ graphs. The exponents shown are a weighted average over the values in Table 3 (corresponding to $A_m = 400$). For comparison, we also included in the table the critical exponents for the Ising model on a flat lattice (the Onsager exponents), for the Ising model coupled dynamically to gravity ($c = 1/2$), and for the Ising model coupled dynamically to gravity and conformal matter with central charge $c_M = -11/2$ (or $c = -5$). Comparing those exponents it is clear that our result agrees very well with the last set of exponents. That the critical behavior agrees so well with the predictions from the KPZ scaling relation for $c = -5$ matter coupled to gravity, strongly supports our conjecture about the effect of disorder on the critical

Table 5. The Critical Exponents of the Ising Model on a Flat Two-Dimensional Lattice (the Onsager Exponents) and Coupled Dynamically to 2*d* Gravity Both for $c = 1/2$ and $c = -5$[a]

	νd_H	$\alpha/\nu d_H$	$\beta/\nu d_H$	$\gamma/\nu d_H$	γ_s	d_H
Onsager	2	log	0.0625	0.875	$-\infty$	2
$c = -5$	2.452...	$-0.184...$	0.0955...	0.809...	$-1.618...$	3.236...
$c = 1/2$	3	$-0.333...$	0.1666...	0.666...	$-0.333...$	4.0–4.2
Quenched	2.464(19)	$-0.27(8)$	0.105(4)	0.793(8)	$-1.5(1)$	3.36(4)

[a] This is compared to the results of our simulations for the Ising model on a quenched ensemble of $c = -5$ graphs. Also shown are the corresponding exponents for the fractal structure of the graphs: γ_s and d_H.

behavior. That is, the dynamical interaction between the matter and the geometry is not important as such, only that they result in a well defined (average) fractal structure for the surfaces.

4. DISCUSSION

The main results of the work presented in this paper can be summarized as follows:

(a) The fractal dimension of surfaces, defined by a conformal field theory with central charge $c = -5$ coupled to two-dimensional quantum gravity, is $d_H = 3.36(4)$. This is in reasonable agreement with, and supports, the theoretical prediction Eq. (19), whereas it definitely rules out Eq. (18).

(b) The critical behavior of an Ising model on a *quenched* ensemble of $c = -5$ graphs agrees well with the predictions, from the KPZ scaling relation, for an Ising model on an *annealed* ensemble of graphs with *identical* fractal properties.

The first result, especially combined with the recent simulations of $2d$-gravity for $c = -2$,[22] lends a strong support to Eq. (19) as a correct description of the fractal structure of two-dimensional quantum gravity for $c \leqslant 0$. This makes, however, its disagreement with numerical simulations in the region $0 < c \leqslant 1$ all the more surprising. What is it in derivation of Eq. (19) that breaks down for $c > 0$? Or are the simulations dominated by finite-size errors and simulations of larger systems will eventually agree with Eq. (19)?

The result for the Ising model is even more interesting. As the theoretical predictions, obtained for an Ising model coupled dynamically to the disorder, agree with our numerical estimate of the critical exponents, our results are consistent with the conjecture put forward in the Introduction that the only thing relevant for the critical behavior of the Ising model are the average fractal properties of graphs the spins "see." We emphasize, however, that this statement is based on a numerical investigation and as such is only valid, of course, within the given numerical accuracy; agreement with Ising models coupled dynamically to other systems with central charge c, in the vicinity of -5, are not ruled out. Further analytical or numerical investigations are needed to corroborate the conjecture.

It is also worth noting that we can continuously change the average fractal properties of the graphs by changing the embedding dimension D in Eq. (3). This allows a continuous interpolation between a flat surface and surfaces corresponding to pure gravity. If the prediction of Liouville theory, the KPZ formula, holds for all those models, this implies that the critical behavior of the Ising model should change continuously in the process. In the language of the renormalization group this implies a continuous line of fixed points, rather than isolated points. There are well known examples of this; the low-temperature phase of the two-dimensional XY-model or the critical line of the Ashkin–Teller model. But is this statement also true for very weak disorder? If we change the fractal dimension infinitesimally, from 2 to $2+\varepsilon$, is that enough to change the critical behavior of the Ising model? Or, alternatively, does there exist some central charge $c' < -5$ were the geometrical disorder is not strong enough and we always get the Onsager exponents? This point deserves further study.

One could also look at the examples of weak disorder that have been studied recently, for example the site or bond-diluted Ising model, and ask if that kind of disorder can also be classified according to some average fractal properties of the lattices. And, moreover, if one could observe some kind of universality in the critical behavior, depending on the fractal structure, akin to what we have presented in this paper.

In view of how dramatically the critical behavior of the Ising model changes on surfaces with such strong disorder, one might ask if such change could be observed in real physical systems. Possible candidates for such systems could be, for example, electrons trapped on the interfaces between two liquids, or on the surface of some porous material, were the surfaces had some well defined non-trivial fractal structure. As our results indicate, it is only the average geometry of the surfaces that is important for the Ising model, not its fluid nature or curvature fluctuations. Thus the relative time-scale between the interactions of the particles and the change in the geometry should be irrelevant.

ACKNOWLEDGMENTS

The work of G.T. was supported by the Humboldt Foundation. The work of P.B. was partially supported by KBN grants 2P03 B19609 and 2P03 B04412.

REFERENCES

1. A. B. Harris, *J. Phys. C* **7**:1671 (1974).
2. Vik. S. Dotsenko and Vl. S. Dotsenko, *J. Phys. C* **15**:495 (1982); *Adv. Phys.* **32**:129 (1983); V. B. Andreichenko, Vl. S. Dotsenko, W. Selke, and J.-S. Wang, *Nucl. Phys. B* **344**:531 (1990); *Europhys. Lett.* **11**:301 (1990); *Physics A* **164**:221 (1990); A. L. Talapov and L. N. Shchure, hep-lat/9404002; J. K. Kim and A. Patrascioiu, *Phys. Rev. Lett.* **72**:2785 (1994).
3. A. W. W. Ludwig, *Nucl. Phys. B* **330**:639 (1990); *Nucl. Phys. B* **285**:97 (1987).
4. V. G. Knizhnik, A. M. Polyakov, and A. B. Zamolodchikov, *Mod. Phys. Lett. A* **3**:819 (1988).
5. C. F. Baillie, K. A. Hawick, and D. A. Johnston, *Phys. Lett. B* **328**:284 (1994); D. A. Johnston, *Phys. Lett. B* **277**:405 (1992).
6. C. F. Baillie, W. Janke, and D. A. Johnston, *Phys. Lett. B* **388**:14 (1996); *Nucl. Phys.* **53**:732 (Proc. Suppl.) (1997).
7. S. Catterall, G. Thorleifsson, M. Bowick, and V. John, *Phys. Lett. B* **354**:56 (1995).
8. J. Ambjørn, J. Jurkiewicz, and Y. Watabiki, *Nucl. Phys. B* **454**:313 (1995).
9. N. Ishibashi and H. Kawai, *Phys. Lett. B* **314**:190 (1993); *Phys. Lett. B* **322**:67 (1994); M. Fukuma. N. Ishibashi, H. Kawai, and M. Ninomiya, *Nucl. Phys. B* **427**:139 (1994); J. Ambjørn, C. F. Kristjansen, and Y. Watabiki, *Nucl. Phys. B* **504**:555 (1997).
10. Y. Watabiki, *Progress in Theoretical Physics*, Suppl. No. 114, p. 1 (1993); H. Kawai, N. Kawamoto, T. Mogami, and Y. Watabiki, *Phys. Lett. B* **306**:19 (1993).
11. P. Ginsparg, Matrix Models of 2d-Gravity, (hep-th/9112013), Lectures given at Trieste Summer School, Trieste, Italy, July 22–25, 1991; L. Alvarez-Gaume, Random Surfaces, Statistical Mechanics and String Theory, *Helv. Phys. Acta* **64**:359 (1991).
12. F. David, Simplicial Quantum Gravity and Random Lattices, (hep-th/9303127), Lectures given at Les Houches Summer School on Gravitation and Quantization, Session LVII, Les Houches, France, 1992; J. Ambjørn, Quantization of Geometry, (hep-th/9411179), Lectures given at Les Houches Summer School on Fluctuating Geometries and Statistical Mechanics, Session LXII, Les Houches, France 1994; P. Di Francesco, P. Ginsparg, and J. Zinn-Justin, *Phys. Rep.* **254**:1 (1995).
13. V. A. Kazakov, *Phys. Lett. A* **119**:140 (1986); D. Boulatov and V. A. Kazakov, *Phys. Lett. B* **186**:379 (1987); Z. Burda and J. Jurkiewicz, *Acta. Phys. Polon. B* **20**:949 (1989).
14. M. Bowick, S. M. Catterall and G. Thorleifsson, *Phys. Lett. B* **391**:305 (1997).
15. J. Ambjørn, G. Thorleifsson, and M. Wexler, *Nucl. Phys. B* **439**:187 (1995).
16. V. A. Kazakov, I. K. Kostov and A. A. Migdal, *Phys. Lett.* **157B**:295 (1985).
17. W. H. Press, S. A. Teukolsky, W. T. Vetterling, and B. P. Flannery, *Numerical Recipes* (Cambrigde University Press, 1992).
18. J. Ambjørn, Ph. De. Forcrand, F. Koukiou, and D. Petritis, *Phys. Lett. B* **197**:548 (1987).
19. S. Jain and S. D. Mathur, *Phys. Lett. B* **286**:239 (1992).
20. J. Ambjørn, S. Jain, and G. Thorleifsson, *Phys. Lett. B* **307**:34 (1993); J. Ambjørn and G. Thorleifsson, *Phys. Lett. B* **323**:7 (1994).

21. J. Ambjørn and K. N. Anagnostopoulos, *Nucl. Phys. B* **497**:445 (1997).
22. N. Kawamoto, V. A. Kazakov, Y. Saeki, and Y. Watabiki, *Nucl. Phys.* **26**:584 (Proc. Suppl.) (1992); *Phys. Rev. Lett.* **68**:2113 (1992); J. Ambjørn, K. N. Anagnostopoulos, T. Ichihara, L. Jensen, N. Kawamoto, Y. Watabiki, and K. Yotsuji, *Phys. Lett. B* **497**:177 (1997); *Nucl. Phys.* (*Proc. Suppl.*) **63**:748 (1998); *Nucl. Phys. B* **511**:673 (1998).
23. P. Bialas, *Phys. Lett. B* **373**:289 (1995); P. Bialas, Z. Burda, and J. Jurkiewicz, *Phys. Lett. B* **421**:86 (1998).
24. J. Ambjørn and Y. Watabiki, *Nucl. Phys. B* **445**:129 (1995).
25. J. Ambjørn, K. N. Anagnostopoulos, U. Magnea, and G. Thorleifsson, *Phys. Lett. B* **388**:713 (1996).
26. M. J. Bowick, V. John, and G. Thorleifsson, *Phys. Lett. B* **403**:197 (1997).
27. J. Ambjørn, K. N. Anagnostopoulos, J. Jurkiewicz, and C. F. Kristjansen, *J. High Energy Phys.* **4**:16 (1998).
28. C. Itzykson and J.-M. Drouffe, *Statistical Field Theory* (Cambridge University Press, Cambridge, 1989).
29. D. Espriu, M. Gross, P. E. L. Rakow, and J. J. Wheater, *Nucl. Phys. B* **265**:92(FS15) (1986); W. Janke, M. Katoot, and R. Villanova, *Phys. Lett. B* **315**:412 (1993); *Phys. Rev. B* **49**:9644 (1994); W. Janke and R. Villanova, *Phys. Lett. A* **201**:179 (1995).
30. V. A. Kazakov, M. Staudacher, and T. Wynter, *Nucl. Phys. B* **471**:309 (1996).
31. A. M. Ferrenberg and R. H. Swendsen, *Phys. Rev. Lett.* **63**:1195 (1989); **61**:2635 (1988).
32. K. Binder and A. P. Young, *Rev. Mod. Phys.* **58**:801 (1986).